MAX-PLANCK-INSTITUT FÜR PHYSIK UND ASTROPHYSIK
WERNER-HEISENBERG-INSTITUT FÜR PHYSIK

MPI-PAE//Exp.El. 199
April 1989

Experimental Test of the PCAC Hypothesis in the Reactions $\nu_\mu p \to \mu^- p\pi^+$ and $\bar{\nu}_\mu p \to \mu^+ p\pi^-$ in the $\Delta(1232)$ Region

Birmingham–CERN–Imperial College–München (MPI)–Oxford–University College Collaboration (WA21)

G.T. JONES, R.W.L. JONES †), B.W. KENNEDY +), S.W. O'NEALE
Department of Physics, University of Birmingham, Birmingham, B15 2TT, UK

D.R.O. MORRISON
CERN, European Laboratory for Particle Physics, CH–1211 Geneva 23, Switzerland

M.M. MOBAYYEN, S. WAINSTEIN
Department of Physics, Imperial College London, London, SW7 2BZ, UK

M. ADERHOLZ, D. HANTKE, E. HOFFMANN, U.F. KATZ, J. KERN, N. SCHMITZ, W. WITTEK
Max–Planck–Institut für Physik und Astrophysik, D–8000 Munich 40, Fed. Rep. of Germany

P. ALLPORT *), G. MYATT, D. RADOJICIC
Department of Nuclear Physics, University of Oxford, Oxford, OX1 3RH, UK

F.W. BULLOCK, S. BURKE *)
Department of Physics and Astronomy, University College London, London, WC1E 6BT, UK

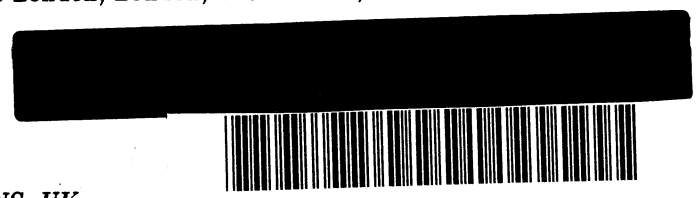

†) *Now at Queen Mary College London, London, E1 4NS, UK*

+) *Now at University College London, London, WC1E 6BT, UK*

*) *Now at Rutherford Appleton Lab., Chilton, Didcot, Oxon, OX11 0QX, UK*

8000 MÜNCHEN 40 - FÖHRINGER RING 6

Experimental Test of the PCAC Hypothesis in the Reactions $\nu_\mu p \to \mu^- p\pi^+$ and $\overline{\nu}_\mu p \to \mu^+ p\pi^-$ in the $\Delta(1232)$ Region

Birmingham–CERN–Imperial College–München (MPI)–Oxford–University College Collaboration (WA21)

G.T. JONES, R.W.L. JONES †), B.W. KENNEDY +), S.W. O'NEALE
Department of Physics, University of Birmingham, Birmingham, B15 2TT, UK

D.R.O. MORRISON
CERN, European Laboratory for Particle Physics, CH–1211 Geneva 23, Switzerland

M.M. MOBAYYEN, S. WAINSTEIN
Department of Physics, Imperial College London, London, SW7 2BZ, UK

M. ADERHOLZ, D. HANTKE, E. HOFFMANN, U.F. KATZ, J. KERN, N. SCHMITZ, W. WITTEK
Max–Planck–Institut für Physik und Astrophysik, D–8000 Munich 40, Fed. Rep. of Germany

P. ALLPORT *), G. MYATT, D. RADOJICIC
Department of Nuclear Physics, University of Oxford, Oxford, OX1 3RH, UK

F.W. BULLOCK, S. BURKE *)
Department of Physics and Astronomy, University College London, London, WC1E 6BT, UK

Submitted to *Zeitschrift für Physik C*

ABSTRACT

Data on the reactions $\nu_\mu p \to \mu^- p\pi^+$ and $\overline{\nu}_\mu p \to \mu^+ p\pi^-$ in the $\Delta(1232)$ region are presented and a test of the PCAC hypothesis, using a modified version of the *Adler* model, is performed. The analysis is based on 1081 events in the neutrino and on 180 events in the antineutrino reaction, obtained in a bubble chamber experiment with BEBC at CERN. The experimental cross–sections for an invariant hadronic mass $W < 1.4$ GeV and an (anti–)neutrino energy $E_\nu^L > 10$ GeV are determined to be $(0.628 \pm 0.059) \cdot 10^{-38}$ cm^2 for the neutrino and $(0.168 \pm 0.023) \cdot 10^{-38}$ cm^2 for the antineutrino reaction. The Q^2 and W distributions, the density matrix elements of the Δ resonance, and moments of the pion angular distribution are discussed. The data are found to be in good agreement with the *Adler* model in the Q^2 region below 1 GeV^2. A maximum likelihood fit for the axial mass m_A in the axial–vector form factor yields a value of $m_A = 1.31 \pm 0.12$ GeV. At low Q^2 the data confirm the PCAC hypothesis and the discrepancy, formerly observed between the experimental and theoretical cross–sections for $\nu_\mu p \to \mu^- p\pi^+$ at low momentum transfers ($Q^2 \lesssim 0.2$ GeV^2), is understood as being due to inadequate pion 'off–mass–shell' corrections.

---

†) *Now at Queen Mary College London, London, E1 4NS, UK*

+) *Now at University College London, London, WC1E 6BT, UK*

*) *Now at Rutherford Appleton Lab., Chilton, Didcot, Oxon, OX11 0QX, UK*

1. Introduction

The concept of a partially conserved axial current (PCAC) [1,2], relating the divergence of the axial current to the pion field operator, was introduced almost 30 years ago; however a detailed experimental investigation of PCAC in high energy (anti–)neutrino reactions has only become possible with the data of the last decade.

In 1964 *Adler* proposed a test of PCAC in (anti–)neutrino nucleon interactions [3]. Some years later he developed a model for weak single–pion production in the Δ resonance region [4], allowing a PCAC test for an invariant hadronic mass $W < 1.4$ GeV. A PCAC test according to [3] for the inclusive reactions $\overset{(-)}{\nu} p \rightarrow \mu^{\pm} X$, based on an extended vector dominance model, can be found in [5,6,7].

As to the weak single–pion production, applications of a simplified version [8] of the *Adler* model in νp [9,10] and νD [11] interactions showed reasonable agreement with experimental data; however at low four–momentum transfer squared ($Q^2 \lesssim 0.2$ GeV^2) the model predictions for the cross–sections were above the experimental data. In some other analyses [12–15], the *Rein–Sehgal* model [16,17], also using PCAC, was applied and yielded similar results. In [9] also a modified version [18] of the *Adler* model was investigated and good agreement with the experimental Q^2 distribution was observed within the large statistical errors.

In the present analysis, data from the WA21 BEBC (**B**ig **E**uropean **B**ubble **C**hamber) experiment for the reactions

$$\nu_\mu p \rightarrow \mu^- p \pi^+ \qquad (1a)$$

$$\overline{\nu}_\mu p \rightarrow \mu^+ p \pi^- \quad , \qquad (1b)$$

with an invariant hadronic mass of $W < 1.4$ GeV are compared to the predictions of the *Adler* model, which has been modified in some respects. For the present analysis the data sample is significantly increased as compared to [10].

This paper is organized as follows: after a brief discussion of the *Adler* model and the modifications performed in the theoretical calculations (section 2), a summary of the experiment and the data selection is given in section 3. The experimental results are presented in section 4 and compared to the model predictions in section 5. For the PCAC test an alternative model for a conserved axial current is compared to the modified *Adler* model in section 6. Finally the conclusions are presented in section 7.

2. Theoretical Concepts

a) DEFINITIONS OF THE KINEMATICAL VARIABLES

The following notations apply to the particles in the reactions (1): k_1, k_2, p_1, p_2 and q are the four–momenta of the (anti–)neutrino, of the muon, of the initial and final proton, and of the pion, respectively. $E_\nu \equiv k_{10}$ and $E_\mu \equiv k_{20}$ are the (anti–)neutrino and muon energies and θ_l is the lepton scattering angle. For the theoretical description it is convenient to choose as reference frame the center of mass system (CMS) of the final hadronic πp state. All variables calculated in this frame carry no index, those in the laboratory system have a superscript 'L'.

From p_1 and the four–momentum transfer $k = k_1 - k_2$ the *Lorentz* invariants $Q^2 = -k_\alpha k^\alpha > 0$ and $W^2 = (p_1 + k)_\alpha (p_1 + k)^\alpha$ are obtained, W being the invariant mass of the final πp system.

In the CMS the direction of motion of the pion can be characterized by the angles θ_π and ϕ_π. The polar angle θ_π is the angle between the pion momentum and the momentum transfer $\vec{k}$, whereas the azimuthal angle ϕ_π is the angle between the projections of the muon momentum vector and the pion momentum vector onto a plane perpendicular to $\vec{k}$ (cf. fig. 1). The lepton plane is spanned by the momentum vectors of the (anti–)neutrino and the muon.

b) THE *ADLER* MODEL

The model by *Adler* [4] describes weak single–pion production in the $\Delta(1232)$ resonance region by a matrix element which is expressed in terms of helicity amplitudes for the vector and axial–vector parts of the weak hadronic current. A partial wave expansion of the matrix element into angular momentum states of the final hadronic system is performed and the helicity amplitudes are calculated in terms of multipole amplitudes, which carry as indices the quantum numbers I (isospin), ℓ (orbital angular momentum) and J (total angular momentum) of the pion–nucleon system. The system of multipoles consists of the vector multipoles $E^I_{\ell\pm}, L^I_{\ell\pm}, M^I_{\ell\pm}$ and the axial–vector multipoles $\mathcal{E}^I_{\ell\pm}, \mathcal{L}^I_{\ell\pm}, \mathcal{M}^I_{\ell\pm}, \mathcal{H}^I_{\ell\pm}$*). The letters $E(\mathcal{E}), L(\mathcal{L}), M(\mathcal{M}), \mathcal{H}$ denote the electric, the longitudinal, the magnetic multipoles and the multipoles which give contributions to the matrix element proportional to the muon mass, respectively.

In the model calculations only s and p partial waves are considered; contributions of higher partial waves are negligible in the W region considered ($W < 1.4$ GeV).

---

*)The subscript '$\ell\pm$' means $J = \ell\pm \equiv \ell \pm 1/2$.

An essential point of the *Adler* model is the explicit calculation of the multipole amplitudes: the nonresonant multipoles are calculated in the *Born* approximation, whereas the resonant multipoles (i. e. the multipoles with the Δ quantum numbers $\ell = 1, I = 3/2, J = 3/2$) are determined using dispersion relations, and are finally related to the resonant partial wave amplitude $f_{1+}^{I=3/2}$ for elastic pion–nucleon scattering with the same quantum numbers.

Form factors are introduced in the calculation of the weak vertices and therefore arise in all multipole expressions. The explicit multipole formulae are given in [4], pp. 297–302. The neutron and proton *Sachs* form factors are fixed using the *scaling law* fit [19], which is consistent with electroproduction data. The axial–vector form factor is written as

$$g_A(Q^2) = \frac{g_A(0)}{(1 + Q^2/m_A^2)^2} \quad , \tag{2}$$

with $g_A(0) = -1.25$ and the axial mass m_A as the only free parameter in the model.

In the theoretical calculations presented in this paper the *Adler* model has been modified in two respects:

- The vector multipoles as functions of Q^2 and W are computed according to a model by *von Gehlen* [20] which is in good agreement with electroproduction data [21, 22]. The original *Adler* model predicts electroproduction cross–sections which are too high for $Q^2 \lesssim 0.2$ GeV^2 and too low for $Q^2 \gtrsim 0.5$ GeV^2 [4, 21, 22]. Using the vector multipole calculations by *von Gehlen* will therefore allow a more reliable determination of m_A.
- The longitudinal axial–vector multipoles are expressed in terms of 'off–mass–shell' pion–nucleon partial wave amplitudes by means of the PCAC hypothesis (see below). In the model used by *Adler* [4] to compare with experimental data, these multipoles are determined by dispersion relations; however also an alternative calculation method is presented in [4], which permits the desired test of PCAC.

A summary of the multipoles and their calculation in the original *Adler* model and in the modified model is given in table 1. The $\mathcal{H}$ multipoles, which give contributions to the matrix element proportional to the muon mass, and some other multipoles (i. e. the Δ multipoles $E_{1+}^{3/2}, L_{1+}^{3/2}$ and $\mathcal{M}_{1+}^{3/2}$ and all multipoles with $I = 1/2$ and $J = 3/2, \ell = 1$) are neglected in the calculations.

c) THE DIFFERENTIAL CROSS–SECTION

The differential cross–section $d\sigma^{\nu,\overline{\nu}}/(dQ^2 dW)$ for the reactions (1) in terms of the multipoles is given by the following formula ([4], p. 215):

$$\frac{d\sigma^{\nu,\overline{\nu}}}{dQ^2 dW} = \frac{G_F^2 \cos^2\theta_c |\overrightarrow{q}|}{2(2\pi)^3 (E_\nu^L)^2} \cdot$$

$$(A) \quad \Big\{ d_1 \sum_\lambda \Big\{ \lambda(\lambda+1)^2 \big[|M^T_{\lambda+}|^2 + |E^T_{(\lambda+1)-}|^2 \big] + \lambda^2(\lambda+1) \big[|M^T_{\lambda-}|^2 + |E^T_{(\lambda-1)+}|^2 \big] \Big\}$$

$$(B) \quad + d_1 \sum_\lambda \Big\{ \lambda(\lambda+1)^2 \big[|\mathcal{M}^T_{(\lambda+1)-}|^2 + |\mathcal{E}^T_{\lambda+}|^2 \big] + \lambda^2(\lambda+1) \big[|\mathcal{M}^T_{(\lambda-1)+}|^2 + |\mathcal{E}^T_{\lambda-}|^2 \big] \Big\}$$

$$(C) \quad + d_2 k_0^2 \sum_\lambda \Big\{ (\lambda+1)^3 |\mathcal{L}^T_{\lambda+}|^2 + \lambda^3 |\mathcal{L}^T_{\lambda-}|^2 \Big\}$$

$$(D) \quad + d_2 \frac{(Q^2)^2}{k_0^2} \sum_\lambda \Big\{ (\lambda+1)^3 |L^T_{(\lambda+1)-}|^2 + \lambda^3 |L^T_{(\lambda-1)+}|^2 \Big\}$$

$$(E) \quad + d_3 \cdot Re \sum_\lambda \Big\{ -\lambda(\lambda+1)^2 (M^T_{\lambda+} \mathcal{E}^{T*}_{\lambda+} + E^T_{(\lambda+1)-} \mathcal{M}^{T*}_{(\lambda+1)-})$$

$$+ \lambda^2(\lambda+1)(M^T_{\lambda-} \mathcal{E}^{T*}_{\lambda-} + E^T_{(\lambda-1)+} \mathcal{M}^{T*}_{(\lambda-1)+}) \Big\} \Big\}, \quad (3)$$

where $G_F = 1.166 \cdot 10^{-5}$ GeV^{-2} is the *Fermi* constant, θ_c is the *Cabibbo* angle and $\vec{q}$ is the pion momentum in the CMS. The coefficients d_1, d_2, d_3 are kinematical functions, given by

$$d_1 = \frac{Q^2}{2}\Big(1 + 2 \cdot \frac{E_\nu E_\mu \cos^2(\theta_l/2)}{|\overrightarrow{k}|^2}\Big)$$

$$d_2 = \frac{2\, E_\nu E_\mu \cos^2(\theta_l/2)}{|\overrightarrow{k}|^2}$$

$$d_3 = \pm \frac{(E_\nu + E_\mu)\, Q^2}{|\overrightarrow{k}|} \quad . \quad (4)$$

The '+' sign in d_3 applies to the neutrino and the '−' sign to the antineutrino reaction. In the summation over the transition order λ of the multipoles in (3) only s and p wave multipoles are considered.

In (3) the isospin summation is already carried out and the multipoles $A^T_{\ell\pm}$ with $A = E, L, M, \mathcal{E}, \mathcal{L}, \mathcal{M}$ are $A^T_{\ell\pm} \equiv c^{1/2} A^{1/2}_{\ell\pm} + c^{3/2} A^{3/2}_{\ell\pm}$. In the reaction $\nu_\mu p \to \mu^- p \pi^+$, $c^{1/2} = 0$ and $c^{3/2} = 1/\sqrt{2}$, whereas in $\overline{\nu}_\mu p \to \mu^+ p \pi^-$ $c^{1/2} = \sqrt{2}/3$ and $c^{3/2} = 1/(3\sqrt{2})$.

The parts (A) to (E) in (3) are the

(A) electric (E) and magnetic (M) vector contributions,

(B) electric ($\mathcal{E}$) and magnetic ($\mathcal{M}$) axial–vector contributions,

(C) longitudinal axial–vector ($\mathcal{L}$) contributions (determined by PCAC in the limit $Q^2 \to 0$),

(D) longitudinal vector (L) contributions,

(E) vector axial–vector interference contributions.

When $Q^2 \to 0$ only term (C) survives (see (4)), so that in this case the cross–section is completely determined by PCAC. The vector parts (A), (D) and the vector axial–vector

interference term (E) vanish at $Q^2 = 0$ as a consequence of the CVC (Conserved Vector Current) hypothesis.

d) THE PCAC HYPOTHESIS AND THE 'OFF–MASS–SHELL' CORRECTION

The PCAC hypothesis [1, 2, 3] relates the divergence of the hadronic axial current $\partial^\alpha A_\alpha$ near $Q^2 = 0$ to the pion field operator Φ_π [23]:

$$\partial^\alpha A_\alpha = f_\pi m_\pi^2 \Phi_\pi \quad , \tag{5}$$

where $f_\pi \simeq 0.932\ m_\pi$ [24] is the pion decay constant and m_π is the pion mass. Applying (5) to the reactions (1) and expanding into partial wave amplitudes one obtains a relation between the longitudinal axial–vector multipoles $\mathcal{L}^T_{\ell\pm}$ and the partial wave amplitudes $f^T_{\ell\pm}$ for elastic pion–nucleon scattering ([4], pp. 206–208):

$$\mathcal{L}^T_{\ell+}(Q^2 = 0) = \frac{8\pi W f_\pi}{\sqrt{2}\cos\theta_c M_p(\ell+1)|\overrightarrow{k}|} \cdot f^T_{\ell+}(Q^2 = 0) \tag{6a}$$

$$\mathcal{L}^T_{\ell-}(Q^2 = 0) = \frac{8\pi W f_\pi}{\sqrt{2}\cos\theta_c M_p \ell\ |\overrightarrow{k}|} \cdot f^T_{\ell-}(Q^2 = 0) \quad , \tag{6b}$$

M_p being the proton mass. Thus the $\mathcal{L}$ multipoles for the reactions (1a) and (1b) are related to the $\pi^+ p$ and $\pi^- p$ scattering amplitudes, respectively. These amplitudes have to be evaluated at $Q^2 > 0$, i. e. for an initial 'off–mass–shell' pion with a mass squared of $-Q^2$, in order to compare the theoretical model to the experimental data. In addition, the $\mathcal{L}$ multipoles at $Q^2 = 0$ are extrapolated to larger Q^2 by multiplying with the axial–vector form factor $(1 + Q^2/m_A^2)^{-2}$ (see (2)).

In the original *Adler* model the off–mass–shell correction is calculated from the threshold behaviour of the partial wave amplitudes in the *Born* approximation $f^{(B)I}_{\ell\pm}$ ([4], p. 207) :

$$\frac{f^I_{\ell\pm\ \mathrm{off}}}{f^I_{\ell\pm\ \mathrm{on}}} \equiv \frac{f^I_{\ell\pm}(-Q^2)}{f^I_{\ell\pm}(m_\pi^2)} \simeq \frac{f^{(B)I}_{\ell\pm}(-Q^2)}{f^{(B)I}_{\ell\pm}(m_\pi^2)} \simeq \frac{|\overrightarrow{k}|^\ell}{|\overrightarrow{q}|^\ell} \quad . \tag{7}$$

Investigations of the reaction $pp \to \Delta^{++} n$, which at low momentum transfer is dominated by single–pion exchange, have shown that (7) yields too large a correction [25]. On the other hand good agreement with experimental data was obtained using the *Dürr–Pilkuhn* off–mass–shell correction [26, 27], which can be written in terms of 'on–shell' and 'off–shell' partial wave amplitudes as

$$\frac{f^{3/2}_{1+\ \mathrm{off}}}{f^{3/2}_{1+\ \mathrm{on}}} = \frac{|\overrightarrow{k}|}{|\overrightarrow{q}|} \cdot \sqrt{\frac{1 + R_\Delta^2 |\overrightarrow{q}|^2}{1 + R_\Delta^2 |\overrightarrow{k}|^2}} \quad . \tag{8}$$

The parameter R_Δ, describing the 'radius' of the Δ vertex, was determined to be 3.97 ± 0.11 GeV^{-1} [28].

In the present analysis this *Dürr–Pilkuhn* correction will be applied for the resonant multipole $\mathcal{L}_{1+}^{3/2}$. Since the contributions of the nonresonant $\mathcal{L}$ multipoles to the differential cross–section are small, their corrections have only small effects and will be calculated according to (7). The amplitudes $f^I_{\ell\pm\ \mathrm{on}}$ have been measured as functions of W and are taken from [29].

In the limit $Q^2 \to 0$, where only the PCAC terms remain, (3) may now be rewritten in terms of the cross–section $\sigma_{\mathrm{off}}(\pi^\pm p \to \pi^\pm p)$ for elastic $\pi^\pm p$ scattering with the initial pion having a mass squared of $-Q^2$. With (6) and using [30]

$$\frac{|\overrightarrow{k}|}{|\overrightarrow{q}|} \cdot \sigma_{\mathrm{off}}(\pi^\pm p \to \pi^\pm p) = 8\pi \cdot \sum_\ell \Big\{ (\ell+1)\Big|f^T_{\ell+}(-Q^2)\Big|^2 + \ell\Big|f^T_{\ell-}(-Q^2)\Big|^2 \Big\} \quad , \qquad (9)$$

one obtains the well–known *Adler* relation between $d\sigma^{\nu,\overline{\nu}}/(dQ^2 dW)$ and the elastic $\pi^\pm p$ cross–section [3]:

$$\left.\frac{d\sigma^{\nu,\overline{\nu}}}{dQ^2 dW}\right|_{Q^2\to 0} = \frac{G_F^2 f_\pi^2 E_\mu^L}{2\pi^2\ |\overrightarrow{k}|\ E_\nu^L} \cdot \sigma_{\mathrm{off}}(\pi^\pm p \to \pi^\pm p) \quad . \qquad (10)$$

In (10) the cross–sections for the reactions '$\overline{\nu}$'$p \to \mu^\mp p \pi^\pm$ are related to the elastic $\pi^\pm p$ cross–sections.

Using the *Goldberger–Treiman* relation $f_\pi \simeq -\sqrt{2}\cos\theta_c M_p g_A(0)/g_r$, where $g_r \simeq 13.5$ [24] is the pion–nucleon coupling constant, one can express the cross–sections for weak single–pion production in terms of $g_A(0)$ and g_r. Inserting the experimental values for $g_A(0) = -1.25$ and g_r will lower the cross–section prediction at $Q^2 = 0$ by approximately 12 %.

e) THE PION ANGULAR DISTRIBUTION

The pion angular distribution in the CMS can be written in terms of the moments $a^{\nu,\overline{\nu}}_{lm}, b^{\nu,\overline{\nu}}_{lm}$ and the spherical harmonics $Y^m_l(\theta_\pi, \phi_\pi)$ in the form

$$\begin{aligned}\frac{d\sigma^{\nu,\overline{\nu}}}{d\Omega_\pi} = \quad & a^{\nu,\overline{\nu}}_{00} Y^0_0 + a^{\nu,\overline{\nu}}_{10} Y^0_1 + a^{\nu,\overline{\nu}}_{20} Y^0_2 \\ & + a^{\nu,\overline{\nu}}_{11} Re Y^1_1 + a^{\nu,\overline{\nu}}_{21} Re Y^1_2 + a^{\nu,\overline{\nu}}_{22} Re Y^2_2 \\ & + b^{\nu,\overline{\nu}}_{11} Im Y^1_1 + b^{\nu,\overline{\nu}}_{21} Im Y^1_2 + b^{\nu,\overline{\nu}}_{22} Im Y^2_2 \quad . \end{aligned} \qquad (11)$$

The relations between the moments $a^{\nu,\overline{\nu}}_{lm}, b^{\nu,\overline{\nu}}_{lm}$ and the multipole amplitudes $E^I_{\ell\pm}, L^I_{\ell\pm}, M^I_{\ell\pm}$ and $\mathcal{E}^I_{\ell\pm}, \mathcal{L}^I_{\ell\pm}, \mathcal{M}^I_{\ell\pm}$ are calculated using the formulae (56), (C.1) to (C.5) in [16] and (A.2.1), (A.2.2) in [31]*).

---

*)Details for the computations of the moments $a^{\nu,\overline{\nu}}_{lm}$ and $b^{\nu,\overline{\nu}}_{lm}$ can be found in [32].

In reaction ($1a$) the nonresonant amplitudes are negligible (cf. section 4b) and the moments $a^{\nu}_{20}, a^{\nu}_{21}, a^{\nu}_{22}$ can be expressed in terms of the density matrix elements $\tilde{\rho}_{33}, \tilde{\rho}_{31}, \tilde{\rho}_{3-1}$ for weak Δ production according to

$$\tilde{\rho}_{33} = \rho_{33} + \rho_{-3-3} = -\frac{\sqrt{5}}{2} \cdot \frac{a^{\nu}_{20}}{a^{\nu}_{00}} + \frac{1}{2} \qquad (12a)$$

$$\tilde{\rho}_{31} = \rho_{31} - \rho_{-1-3} = \frac{\sqrt{10}}{4} \cdot \frac{a^{\nu}_{21}}{a^{\nu}_{00}} \qquad (12b)$$

$$\tilde{\rho}_{3-1} = \rho_{3-1} + \rho_{1-3} = -\frac{\sqrt{10}}{4} \cdot \frac{a^{\nu}_{22}}{a^{\nu}_{00}} \quad . \qquad (12c)$$

In this case the usual formula [10] for the angular decay distribution of the Δ resonance

$$\frac{d\sigma^{\nu}}{d\Omega_{\pi}} = \frac{\sigma^{\nu}}{2\sqrt{\pi}} \cdot \left\{ Y^0_0 - \frac{2}{\sqrt{5}}(\tilde{\rho}_{33} - \frac{1}{2}) Y^0_2 + \frac{4}{\sqrt{10}} \tilde{\rho}_{31} Re Y^1_2 - \frac{4}{\sqrt{10}} \tilde{\rho}_{3-1} Re Y^2_2 \right\} \qquad (13)$$

is obtained.

3. Experiment and Data Selection

a) EXPERIMENTAL DETAILS

The experiment was carried out in the period 1977 to 1983 with the BEBC bubble chamber [33], which was exposed in four different runs to the (anti-)neutrino wideband beam [34] of the CERN SPS. The bubble chamber was filled with approximately 30 m^3 of liquid hydrogen and kept in a vertical magnetic field of 3.5 T. Electronic components of the detector were the **E**xternal **M**uon **I**dentifier (EMI) [35] and the **I**nternal **P**icket **F**ence (IPF) [36], which was installed in 1981.

The BEBC volume was photographed in 4 different stereoscopic views and the photographs were scanned with a scanning efficiency of 95 $\pm$ 2 % for events with 3 charged secondary particles. The events were geometrically reconstructed and the tracks were extrapolated to the EMI planes. The geometrical acceptance of the EMI varied from 40 % at $E^L_{\mu} = 3$ GeV to 100 % for $E^L_{\mu} > 10$ GeV.

b) THE EVENT SELECTION

For the selection of the events belonging to the desired reaction classes (1) the following cuts are applied:

- The primary vertex is required to lie in a fiducial volume of about 19 m^3 to allow accurate track reconstruction and determination of the particle momenta.

- A muon energy cut is performed requiring the events to have a laboratory muon energy $E_\mu^L > 3$ GeV. This allows a reliable muon identification and the separation of a background of reactions induced by neutral hadrons. In the analysis, events with muons, that have no EMI identification and are only identified by a kinematic fit are also considered, however 97.4 % of the finally analysed neutrino and all antineutrino events are identified by the EMI.
- Only events with an acceptable kinematic fit to the reaction hypotheses (1) are considered. The χ^2 probability for this fit is required to be larger than 2 %, in order to exclude false fits, mainly due to additional unseen neutral particles. After this cut the distributions of the probability $P(\chi^2)$ are flat for both reactions [32]. Among the remaining neutrino events there are 4 events which have two fits. For these events the fit with the highest probability is accepted.
- There is evidence for losses of events in which the final proton has a low momentum $p_p^L \lesssim 0.2$ GeV/c. Such slow protons are unlikely to be observed in the bubble chamber because of their short track length. Since Q^2 and p_p^L are correlated, this introduces small biases in the Q^2 distributions. From the angular distribution of the outgoing proton momentum around the beam axis in the laboratory system, from the distribution of the vertical vertex coordinate, and from a comparison between the theoretically predicted and the observed p_p^L distributions, the losses are estimated to be 10 ± 5 events for $Q^2 < 0.1$ GeV^2 in the neutrino reaction. For the antineutrino reaction with much larger statistical errors, losses of this kind are assumed to be negligible. In the neutrino reaction, the experimental values for the moments of the pion angular distribution (cf. section 4b) and for the differential cross–section $d\sigma^\nu/dQ^2$ (cf. section 6) have been corrected for these losses. In the comparison between the experimental and theoretical Q^2 distributions (cf. section 5), p_p^L is required to be larger than 0.2 GeV/c. The tracks of such protons are sufficiently long to be observed on the bubble chamber photographs.

The final data sample (uncorrected for losses) contains 1494 neutrino events and 609 antineutrino events with an invariant mass $W < 3$ GeV. In the region $W < 1.4$ GeV, which is discussed in this paper, there are 1081 events in the neutrino reaction and 180 events in the antineutrino reaction. The mean (anti–)neutrino energies for these events are 25 and 26.8 GeV, respectively. A summary of the important cuts and the remaining events is given in table 2.

4. Experimental Results

a) THE DISTRIBUTIONS OF W AND Q^2

The mean measurement errors of W and Q^2 are estimated to be $\Delta W \simeq 0.006$ GeV and $\Delta Q^2 \simeq 0.01$ GeV^2 respectively. Therefore the chosen interval widths of 0.02 GeV for the W and of 0.05 GeV^2 for the Q^2 distribution in the neutrino reaction ensure that smearing in these variables due to experimental uncertainties is negligible. In the antineutrino reaction twice these interval widths are taken in order to lower the relative statistical errors.

The W distributions for $W < 3$ GeV are shown in fig. 2. In the reaction ($1a$) the distribution is dominated by the $\Delta(1232)$ resonance, whereas in the antineutrino reaction there is evidence for additional resonances in the region 1.4 GeV $< W <$ 1.8 GeV. The present analysis will be restricted to the interval $W < 1.4$ GeV, which is dominated by the production of the $\Delta(1232)$ resonance. Results for the region $W > 1.4$ GeV can be found in [13].

The Q^2 distributions for $W < 1.4$ GeV are shown in fig. 3. The black areas show the number of events which fall in the range $p_p^L < 0.2$ GeV/c. The remaining events have a proton momentum $p_p^L > 0.2$ GeV/c.

b) THE MOMENTS OF THE PION ANGULAR DISTRIBUTION

In order to determine the moments $a_{lm}^{\nu,\overline{\nu}}, b_{lm}^{\nu,\overline{\nu}}$ of the pion angular distribution in the CMS several experimental methods are applied:

1) The method of moments, by which $a_{lm}^{\nu,\overline{\nu}}$ and $b_{lm}^{\nu,\overline{\nu}}$ are calculated using the mean values of the spherical harmonics $Y_l^m(\theta_\pi, \phi_\pi)$, and
2) the method of asymmetries, by which the moments are obtained from the differences of the numbers of events in different $(\Delta \cos\theta_\pi, \Delta\phi_\pi)$ regions.
3) Additionally, for the neutrino reaction, a maximum likelihood fit of (13) to the ($\cos\theta_\pi$, ϕ_π) distribution is performed, with the density matrix elements as free parameters.

In the neutrino reaction the three methods yield very similar results. Therefore only the data obtained in applying the method of moments, being the most general method, will be presented in the analysis. The agreement of methods 1) and 3) suggests that in reaction ($1a$) the nonresonant background is small and therefore the relations (12) can be applied.

For the neutrino channel the moments are determined in five Q^2 intervals with $Q^2 <$ 1 GeV^2, chosen such that they contain similar numbers of events (cf. table 3). In the first interval $Q^2 < 0.1$ GeV^2 a correction for the losses described in 3b) has been applied. A theoretical calculation of the angular distribution shows that these losses are restricted

to the region $\cos\theta_\pi > 0.5$. The corrected values for a^ν_{lm} and b^ν_{lm} are determined as the averages of the values obtained after adding 10 events with $\cos\theta_\pi = 0.5$ and $\cos\theta_\pi = 1.0$, respectively. The difference between the two results is taken into account in calculating the statistical errors. Table 3 shows the density matrix elements $\tilde{\rho}_{33}, \tilde{\rho}_{31}, \tilde{\rho}_{3-1}$ and table 4 the moments $a^\nu_{10}, a^\nu_{11}, b^\nu_{11}, b^\nu_{21}, b^\nu_{22}$ for the neutrino reaction $(1a)$. The asymmetry of the $\cos\theta_\pi$ distribution is found to be positive ($a^\nu_{10} > 0$).

The main moments $a^{\overline{\nu}}_{20}, a^{\overline{\nu}}_{21}, a^{\overline{\nu}}_{22}$ in the antineutrino reaction $(1b)$, calculated from 126 events with $Q^2 < 1$ GeV^2, are given in table 5. Within one standard deviation the two methods used yield identical results.

c) THE EXPERIMENTAL CROSS-SECTIONS

The cross-sections $\sigma^{\nu,\overline{\nu}}(E^L_\nu)$ for the reactions (1) with $W < 1.4$ GeV are determined from the total charged current '$\overline{\nu}$'p cross-sections $\sigma^{\nu,\overline{\nu}}_{\rm tot}(E^L_\nu) = \sigma^{\nu,\overline{\nu}}_0 \cdot E^L_\nu$ using

$$\frac{n^{\nu,\overline{\nu}}_{\rm tot}(E^L_\nu)}{\sigma^{\nu,\overline{\nu}}_{\rm tot}(E^L_\nu)} = \frac{n^{\nu,\overline{\nu}}(E^L_\nu)}{\sigma^{\nu,\overline{\nu}}(E^L_\nu)} \quad . \tag{14}$$

$n^{\nu,\overline{\nu}}_{\rm tot}(E^L_\nu)$ and $n^{\nu,\overline{\nu}}(E^L_\nu)$ are the (anti-)neutrino energy distributions dN/dE^L_ν for the total charged current event sample and for reactions (1) with $W < 1.4$ GeV, respectively. The values for $n^{\nu,\overline{\nu}}_{\rm tot}(E^L_\nu)$ are taken from [7], where the same data sample is used.

Integrating (14) for $E^L_\nu > 10$ GeV, and assuming $\sigma^{\nu,\overline{\nu}}(E^L_\nu) \equiv \sigma^{\nu,\overline{\nu}}$ to be constant in this energy range [13] yields

$$\frac{1}{\sigma^{\nu,\overline{\nu}}_0} \cdot \int\limits_{E^L_\nu > 10\ \rm GeV} dE^L_\nu \, \frac{n^{\nu,\overline{\nu}}_{\rm tot}(E^L_\nu)}{E^L_\nu} = \frac{N^{\nu,\overline{\nu}}}{\sigma^{\nu,\overline{\nu}}} \quad , \tag{15}$$

where $N^{\nu,\overline{\nu}}$ are the numbers of events for the reactions (1) in the region $W < 1.4$ GeV and $E^L_\nu > 10$ GeV. Using the latest measurements [37] of $\sigma^{\nu,\overline{\nu}}_0$ with $\sigma^\nu_0 = (0.474 \pm 0.029) \cdot 10^{-38}$ cm^2/GeV and $\sigma^{\overline{\nu}}_0 = (0.500 \pm 0.032) \cdot 10^{-38}$ cm^2/GeV, values of $\sigma^\nu = (0.628 \pm 0.059) \cdot 10^{-38}$ cm^2 and $\sigma^{\overline{\nu}} = (0.168 \pm 0.023) \cdot 10^{-38}$ cm^2 are obtained. These cross-sections contain corrections for scanning losses (5 ± 2 %), for the $P(\chi^2)$ cut (2 %), and for the losses of events with slow protons (1 %). The errors quoted include the one standard deviation uncertainty of $\sigma^{\nu,\overline{\nu}}_0$, the statistical error of $N^{\nu,\overline{\nu}}$ and the uncertainty of the scanning losses.

5. Comparison of the Data with the Model Predictions

a) CALCULATION OF THE THEORETICAL PREDICTIONS

In order to minimize the statistical errors and to allow for the most accurate test of the theory, the model prediction for the cross–section is transformed to number of events according to

$$\Delta N_{\rm th}^{\nu,\overline{\nu}} = \int_{\Delta E_\nu^L} dE_\nu^L \frac{n^{\nu,\overline{\nu}}(E_\nu^L)}{\sigma_{\rm exp}^{\nu,\overline{\nu}}(E_\nu^L)} \int_{\Delta W} dW \int_{\Delta Q^2} dQ^2 \int_{\Delta\Omega_\pi} d\Omega_\pi \frac{d\sigma_{\rm th}^{\nu,\overline{\nu}}(E_\nu^L)}{dW dQ^2 d\Omega_\pi} \quad , \qquad (16)$$

where $\Delta N_{\rm th}^{\nu,\overline{\nu}}$ denotes the model prediction for the number of events in a $\Delta W \Delta Q^2 \Delta\Omega_\pi$ interval. $\sigma_{\rm th}^{\nu,\overline{\nu}}$ (from (3)), and $\sigma_{\rm exp}^{\nu,\overline{\nu}}$ (from (14)) are the theoretical and experimental cross–sections of reactions (1) for $W < 1.4$ GeV, respectively. The experimental cross–sections for (1), determined for $E_\nu^L > 10$ GeV as described in section 4c), have been extrapolated to lower E_ν^L assuming a threshold behaviour of the cross–sections as given by the *Adler* model (for details see [32]).

b) THE DETERMINATION OF THE AXIAL MASS m_A

The axial mass m_A in the axial–vector form factor (2) is determined by a simultaneous maximum likelihood fit of the predicted Q^2 distributions for (1) to the experimental Q^2 distributions in the region $Q^2 < 1$ GeV^2. The result of this fit is $m_A = 1.31 \pm 0.12$ GeV with a χ^2 per degree of freedom of $25.4/18 = 1.41$ in the neutrino reaction and $7.29/8 = 0.91$ in the antineutrino reaction. In all subsequent theoretical calculations this value of m_A is used. The fitted Q^2 distributions are shown by the curves in fig. 4, together with and normalized to the experimental data. It should be noted that the result of m_A depends on the values of the vector multipoles and is also sensitive to replacing f_π with the experimental values of $g_A(0)$ and g_r (cf. section 1d). Using $g_A(0) = -1.25$ and $g_r = 13.5$, a value of $m_A = 1.25 \pm 0.12$ GeV is obtained.

Table 6 gives a compilation of m_A values obtained in various analyses. The results range from 0.85 to 1.43 GeV, the differences being due to different models that were applied in the analyses, different experimental input, and to different experimental quantities being used to determine m_A.

c) EXPERIMENTAL AND THEORETICAL Q^2 AND W DISTRIBUTIONS

In fig. 5 the experimental Q^2 distributions are compared to absolute predictions of the four following models:

A: the model presented in this paper with the *Dürr–Pilkuhn* pion 'off–mass–shell' correction (8) for the resonant multipole $\mathcal{L}_{1+}^{I=3/2}$ and the *Adler* corrections (7) for the nonresonant $\mathcal{L}$ multipoles,

B: the model including the 'off–mass–shell' corrections according to the original *Adler* model (7),

C: the model without 'off–mass–shell' corrections (i. e. $f^I_{\ell\pm\ \mathrm{off}} \equiv f^I_{\ell\pm\ \mathrm{on}}$), and

D: an alternative model for a 'conserved axial current' (CAC) without the longitudinal $\mathcal{L}$ multipoles, i. e. without PCAC (cf. section 6).

In the neutrino reaction the agreement of the models A and C with the data is good, whereas the model B is above the experimental points for $Q^2 \lesssim 0.2$ GeV^2. The alternative model D is discussed in detail in section 6, where it is compared to the modified *Adler* model A. In the antineutrino channel all model predictions are in good agreement with the experimental data.

Fig. 6 shows the contributions of the longitudinal axial–vector, of the vector and of the remaining axial–vector parts to the predicted Q^2 distributions according to model A. The longitudinal axial–vector multipoles, which are determined by PCAC in the limit $Q^2 \to 0$, contribute only for $Q^2 \lesssim 0.2$ GeV^2. The vector parts are dominant for $Q^2 \gtrsim 0.6$ GeV^2 in the neutrino and for $Q^2 \gtrsim 0.4$ GeV^2 in the antineutrino reaction.

In fig. 7 the contributions of the various angular momentum channels $\ell\pm$ to the predicted Q^2 distributions according to model A are shown. After integrating over the Q^2 range the nonresonant background from the 0+ and 1− partial waves amounts to approximately 7% of the total distribution in the neutrino channel, whereas in the antineutrino reaction a large background of 57% contributes to the Q^2 distribution.

In fig. 8 the experimental W distributions are compared with the theoretical W distributions, which have been normalized to the experimental data. The shapes are in good agreement, with a χ^2/NDF of $18/15 = 1.20$ in the neutrino reaction and of $1.9/7 = 0.27$ in the antineutrino reaction. The resonance behaviour of the cross–section reflects the resonance behaviour of the $(I = 3/2, \ell\pm = 1+)$ pion–nucleon partial wave, which is contained in the corresponding multipoles.

d) DENSITY MATRIX ELEMENTS AND MOMENTS $a_{lm}^{\nu,\overline{\nu}}, b_{lm}^{\nu,\overline{\nu}}$

The density matrix elements for the $\Delta^{++}(1232)$ in the neutrino reaction, calculated from the experimental angular distribution of the pion, and the corresponding theoretical predictions are displayed in fig. 9. The experimental values for the matrix elements are in good agreement with the theoretical predictions of the modified model A including PCAC.

The alternative model D (CAC, dashed lines), which is discussed in section 6, fails to describe the experimental data.

The remaining moments of the pion angular distribution in the neutrino reaction are shown in fig. 10. In general these data are compatible with the theory, however the differences between CAC and PCAC are too small to distinguish between the two models. Due to the large experimental errors in the antineutrino reaction the data are not conclusive and will therefore not be discussed.

6. Test of the Models with and without the $\mathcal{L}$ Multipoles

For a test of the PCAC hypothesis, the two models A and D are compared with the data:

- the modified *Adler* model including the longitudinal axial–vector multipoles $\mathcal{L}^I_{\ell\pm}$, which are determined by PCAC, and including the *Dürr–Pilkuhn* 'off–mass–shell' corrections as described in section 2 (model A),
- the *Adler* model without the longitudinal axial–vector multipoles. If these multipoles are left out, the cross–section vanishes for $Q^2 \to 0$ as predicted by a theory of a 'conserved axial current' (CAC, model D).

For the lowest bin ($0 < Q^2 < 0.05$ GeV^2) of the Q^2 distribution in the neutrino reaction the modified model A describes the data well, while the CAC prediction (model D) differs from the data by more than 4 standard deviations (cf. fig. 5). Significant differences between the two models show up also in the predictions for the density matrix element $\tilde{\rho}_{31}$. This density matrix element is proportional to the PCAC multipole amplitude $\mathcal{L}^{3/2}_{1+}$ and is therefore very sensitive to a variation of this amplitude. As is seen in fig. 9 the data are in good agreement with the modified model A, and they clearly disagree with a value of zero as predicted by the alternative model D.

In order to quantify the comparison in shape and absolute value between the data and the model predictions, χ^2 values are calculated taking into account two kinds of errors:

- the statistical errors in the experimental distributions and
- the errors of the experimental total charged current '$\bar{\nu}p$' cross–sections in the theoretical predictions (cf. (16, 14)).

The influence of the latter error on the predicted Q^2 distributions is indicated in fig. 11, where the shaded areas show the one standard deviation uncertainty of the theoretical predictions.

Because the $\mathcal{L}$ multipoles contribute only at low $Q^2 (\lesssim 0.2$ GeV$^2)$, only the lowest three Q^2 bins in each distribution are used for calculating the χ^2 values. A summary of the χ^2 values obtained is given in table 7, indicating good agreement between the predictions of

the modified *Adler* model A and the experimental data (χ^2 per degree of freedom near 1 or less). The alternative model D yields much higher χ^2 values, especially for $\tilde{\rho}_{31}$ and the Q^2 distribution in the neutrino reaction, and can be excluded at a high confidence level.

The Q^2 distributions are also transformed into the differential cross–sections $d\sigma^{\nu,\overline{\nu}}/dQ^2$ by weighting the events with $\sigma^{\nu,\overline{\nu}}_{\rm exp}(E^L_\nu)/n^{\nu,\overline{\nu}}(E^L_\nu)$ (cf. fig. 12). As a consequence, the relative statistical errors are somewhat larger than in the experimental Q^2 distributions in terms of events dN/dQ^2 as presented in figs. 4, 5. In contrast to these figures, in fig. 12 no proton momentum cut was applied, instead in the neutrino reaction 7 events in the first and 3 events in the second bin were added to correct for the losses described in section 3b). The theoretical predictions for $d\sigma^{\nu,\overline{\nu}}/dQ^2$ are calculated at the mean values of the (anti–)neutrino energies in reactions (1).

7. Conclusions

The experimental data for the reactions $\nu_\mu p \rightarrow \mu^- p\pi^+$ and $\overline{\nu}_\mu p \rightarrow \mu^+ p\pi^-$ in the invariant hadronic mass region $W < 1.4$ GeV have been analysed. The experimental cross–sections for these reactions were determined to be $(0.628 \pm 0.059) \cdot 10^{-38}$ cm^2 in the neutrino and $(0.168 \pm 0.023) \cdot 10^{-38}$ cm^2 in the antineutrino channel for $E^L_\nu > 10$ GeV. The experimental data have been compared to the theoretical predictions of a modified version of the *Adler* model [4]. The longitudinal axial–vector multipoles $\mathcal{L}^I_{\ell\pm}$ were related to partial wave amplitudes for elastic pion–nucleon scattering by means of the PCAC hypothesis. For a determination of the axial mass m_A in the axial–vector form factor a simultaneous maximum likelihood fit of the predicted normalized Q^2 distributions in both reactions to the experimental data was performed, yielding a value of $m_A = 1.31 \pm 0.12$ GeV. The Q^2 distributions in both reactions and the density matrix elements for the neutrino reaction were found to be in good agreement with the theoretical predictions. At low Q^2 the data confirm the PCAC hypothesis. An alternative model with a conserved axial current (CAC) can be excluded at a high confidence level. The discrepancy in the Q^2 distributions at low Q^2 between the original *Adler* model predictions and the data, as observed in [10] and in this paper, can be removed by using *Dürr–Pilkuhn* 'off–mass–shell' corrections [26], already proved successful in pion exchange reactions [25, 28].

We gratefully thank the scanning and measuring crews of our laboratories for their accurate and careful work. We thank the staff at CERN and the BEBC, IPF and EMI groups. In some intricate theoretical questions, a discussion with Wolfgang Ochs was of great benefit.

REFERENCES

[1] Y. Nambu, *Phys. Rev. Lett.* **4**, 380 (1960)

[2] M. Gell–Mann, M. Lévy, *Nuovo Cim.* **16**, 705 (1960)

[3] S. L. Adler, *Phys. Rev.* **135**, B963 (1964)

[4] S. L. Adler, *Ann. of Phys.* **50**, 189 (1968)

[5] P. Allport, Ph.D. Thesis, Oxford (1986)

[6] U. F. Katz, Diploma thesis, München (1986)

[7] G. T. Jones et al., *Z. Phys.* **C 37**, 25 (1987)

[8] P. A. Schreiner, F. von Hippel, *Phys. Rev. Lett.* **30**, 339 (1973); *Nucl. Phys.* **B58**, 333 (1973)

[9] J. Bell et al., *Phys. Rev. Lett.* **41**, 1012 (1978)

[10] P. Allen et al., *Nucl. Phys.* **B 176**, 269 (1980)

[11] T. Kitagaki et al., *Phys. Rev.* **D 34**, 2554 (1986)

[12] D. Allasia et al., *Z. Phys.* **C 20**, 95 (1983)

[13] P. Allen et al., *Nucl. Phys.* **B 264**, 221 (1986)

[14] H. J. Grabosch et al., *Z. Phys.* **C 41**, 527 (1989)

[15] H. J. Grabosch et al., *Cross–Section Measurement for the reaction* $\nu p \rightarrow \mu^- p \pi^+$ *in the Energy range below 30* GeV, SKAT–Collaboration, Inst. f. Hochenergiephysik, Akad. d. Wissenschaften der DDR, Berlin–Zeuthen (1987), Preprint PHE 87–06

[16] D. Rein, *Z. Phys.* **C 35**, 43 (1987)

[17] D. Rein, L. M. Sehgal, *Ann. of Phys.* **133**, 79 (1981)

[18] S. L. Adler, *Phys. Rev.* **D 12**, 2644 (1975)

[19] M. Goitein et al., *Phys. Rev. Lett.* **18**, 1018 (1967)

[20] G. von Gehlen, *Nucl. Phys.* **B 9**, 17 (1969); *Nucl. Phys.* **B 20**, 102 (1970)

[21] K. Bätzner et al., *Phys. Lett.* **B 39**, 575 (1972)

[22] W. Bartel et al., *Phys. Lett.* **B 35**, 181 (1971)

[23] P. Roman: *Introduction to Quantum Field Theory*, Wiley, New York (1969)

[24] G. Ebel et al., *Springer Tracts in Mod. Phys.* **55**, 239 (1970)

[25] G. Wolf, *Phys. Rev.* **182**, 1538 (1969)

[26] H. P. Dürr, H. Pilkuhn, *Nuovo Cim.* **40 A**, 899 (1965)

[27] P. E. Schlein: *Review of Experimental Results on the $\pi\pi$ and $K\pi$ Interactions*, Lecture notes for the Int. School of Subnuclear Physics, 'Elementary Processes at High Energy', Erice, Sicily, July 1970

[28] G. Wolf, *Phys. Rev. Lett.* **19**, 925 (1967)

[29] R. A. Arndt, J. M. Ford, L. D. Roper, *Phys. Rev.* **D 32**, 1085 (1985)

[30] B. H. Bransden, R. G. Moorhouse: *The Pion–Nucleon System*, Princeton University Press, New Jersey (1973)

[31] D. Rein, *Ein–Pion–Erzeugung in Neutrino–Reaktionen*, RWTH Aachen (1986)

[32] D. Hantke, Diploma thesis, München (1988)

[33] G. Harigel, *BEBC Users Handbook*, CERN (1977)

[34] H. W. Wachsmuth, *Physics of Neutrino Beams*, Weak Interactions (Enrico Fermi School), Varenna (1979); W. A. Venus, H. W. Wachsmuth, *Remarks on Neutrino Fluxes and their Measurement in 200 and 400 GeV Neutrino Experiments Using Wide Band and Narrow Band Beams*, int. CERN–Report TCL/73–2 (1973)

[35] C. Brand et al., *Nuc. Inst. Meth.* **136**, 485 (1976); R. Beuselinck et al., *Nuc. Inst. Meth.* **154**, 445 (1978)

[36] H. Foeth, *Nuc. Inst. Meth.* **176**, 203 (1980); M. L. Retter, S. J. Towers, *The Internal Picket Fence Detector*, Nuclear Physics Laboratory, Oxford, Ref. 25/85 (1985); H. Foeth et al., *Nuc. Inst. Meth.* **A253**, 245 (1987)

[37] M. Aderholz et al., *Phys. Lett.* **B 173**, 211 (1986)

Table 1: Method of calculating the multipoles.

The abbreviations denote respectively: '$-$' unphysical multipoles, 'd' multipoles calculated by solving dispersion relations, 'B' multipoles calculated in the *Born* approximation, 'n' neglected multipoles, 'G' vector multipoles determined according to *von Gehlen*, 'P' multipoles determined by PCAC. Whenever the modified model differs from the original model, used by *Adler* to compare with experimental data, the original determination is indicated in square brackets. The column with a star contains the resonant multipoles. I denotes the isospin, ℓ the orbital angular momentum of the πp system and $\ell\pm$ means $J = \ell \pm 1/2$, where J is the πp total angular momentum.

	$I = 3/2$			$I = 1/2$		
$\ell\pm$	0+	1+*)	1−	0+	1+	1−
M	−	$G[d]$	$G[B]$	−	$n[B]$	$G[B]$
E	$G[B]$	$n[d]$	−	$G[B]$	$n[B]$	−
L	$G[B]$	$n[d]$	$G[B]$	$G[B]$	$n[B]$	$G[B]$
$\mathcal{M}$	B	$n[d]$	−	B	$n[B]$	−
$\mathcal{E}$	−	d	B	−	$n[B]$	B
$\mathcal{L}$	$P[B]$	$P[d]$	$P[B]$	$P[B]$	$n[B]$	$P[B]$
$\mathcal{H}$	$n[P]$	$n[P]$	$n[P]$	$n[P]$	$n[P]$	$n[P]$

Table 2: Statistics of the event selection.

selection criteria	number of events remaining after cuts	
	νp	$\overline{\nu} p$
fiducial volume	21015	14285
$E_\mu^L > 3$ GeV	7032	6324
(events with EMI-identified $\mu^\mp$)	(6986)	(6322)
fit events to (1) with $P(\chi^2) > 2$ %	1558	684
$W < 1.4$ GeV	1081	180
$p_p^L > 0.2$ GeV/c	1072	178

Table 3: Density matrix elements for νp determined by the method of moments.

The sample of 155 events in the first Q^2 bin consists of 137 events with $p_p^L > 0.2$ GeV/c, 8 observed events with $p_p^L < 0.2$ GeV/c and 10 events added to correct for the losses at $p_p^L < 0.2$ GeV/c.

Q^2 (GeV^2)	$\tilde{\rho}_{33}$	$\tilde{\rho}_{31}$	$\tilde{\rho}_{3-1}$
$0. - 0.1$ (155 events)	0.44 ± 0.08	-0.33 ± 0.13	-0.08 ± 0.09
$0.1 - 0.2$ (145 events)	0.86 ± 0.08	-0.24 ± 0.09	-0.23 ± 0.10
$0.2 - 0.4$ (218 events)	0.79 ± 0.07	-0.11 ± 0.07	-0.15 ± 0.08
$0.4 - 0.6$ (175 events)	0.61 ± 0.08	0.03 ± 0.08	-0.06 ± 0.09
$0.6 - 1.0$ (186 events)	0.76 ± 0.07	0.10 ± 0.08	-0.03 ± 0.09

Table 4: Moments $a^\nu_{10}, a^\nu_{11}, b^\nu_{11}, b^\nu_{21}, b^\nu_{22}$ for νp determined by the method of moments.

Q^2 (GeV^2)	a^ν_{10}/a^ν_{00}	a^ν_{11}/a^ν_{00}	b^ν_{11}/a^ν_{00}	b^ν_{21}/a^ν_{00}	b^ν_{22}/a^ν_{00}
$0. - 0.1$	0.19 ± 0.09	-0.08 ± 0.12	0.13 ± 0.11	-0.14 ± 0.12	0.01 ± 0.11
$0.1 - 0.2$	0.07 ± 0.07	-0.02 ± 0.13	0.15 ± 0.12	0.20 ± 0.10	-0.11 ± 0.13
$0.2 - 0.4$	0.07 ± 0.06	-0.06 ± 0.11	0.25 ± 0.09	0.02 ± 0.09	0.02 ± 0.10
$0.4 - 0.6$	0.16 ± 0.07	-0.15 ± 0.11	0.14 ± 0.11	0.06 ± 0.10	-0.18 ± 0.11
$0.6 - 1.0$	0.14 ± 0.06	0.00 ± 0.11	0.21 ± 0.11	0.01 ± 0.10	0.14 ± 0.11

Table 5: Moments $a^{\overline{\nu}}_{20}, a^{\overline{\nu}}_{21}, a^{\overline{\nu}}_{22}$ for $\overline{\nu}p$ with $Q^2 < 1$ GeV^2.

	$a^{\overline{\nu}}_{20}/a^{\overline{\nu}}_{00}$	$a^{\overline{\nu}}_{21}/a^{\overline{\nu}}_{00}$	$a^{\overline{\nu}}_{22}/a^{\overline{\nu}}_{00}$
method of moments :	-0.06 ± 0.09	-0.16 ± 0.12	0.00 ± 0.12
method of asymmetries :	-0.13 ± 0.10	-0.27 ± 0.15	0.03 ± 0.15

Table 6: Values of m_A obtained in various analyses.

The abbreviations denote respectively: '$MA1$','$MA2$' modified versions of the *Adler* model [4, 18], 'SvH' the *Schreiner–von–Hippel* parametrization [8] of the *Adler* model, 'RS' the *Rein–Sehgal* model [16, 17]. In all the analyses except for [14, 15], the invariant mass W was required to be less than 1.4 GeV.

reference	model	value of m_A (GeV)	fitted quantity	reaction
[9]	$MA1$	$1.25^{+0.15}_{-0.13}$	Q^2 distribution, $Q^2 < 1$ GeV^2	$\nu p \to \mu^- p\pi^+$
		$1.43^{+0.07}_{-0.09}$	Q^2 distribution, $Q^2 < 3$ GeV^2	
	SvH	1.15 ± 0.10	Q^2 distribution, $Q^2 < 3$ GeV^2	
[10]	SvH	0.85 ± 0.10	$\sigma(E_\nu^L)$	$\nu p \to \mu^- p\pi^+$
[11]	SvH	1.28 ± 0.11	Q^2 distribution, 0.1 GeV$^2 < Q^2 < 3$ GeV^2	$\nu D \to \mu^- p\pi^+(n)$
[12]	RS	0.96 ± 0.08	$\sigma(E_\nu^L)$	$\overline{\nu} D \to \mu^+ p\pi^-(n)$, $\overline{\nu} D \to \mu^+ n\pi^-(p)$
[14, 15]	RS	1.01 ± 0.10	$\sigma(E_\nu^L), W < 1.6$ GeV	$\nu p \to \mu^- p\pi^+$
[14]	RS	1.05 ± 0.09	$\sigma(E_\nu^L), W < 2$ GeV	$\overline{\nu} p \to \mu^+ p\pi^-$
this analysis	$MA2$	1.31 ± 0.12	Q^2 distribution, $Q^2 < 1$ GeV^2	$\nu p \to \mu^- p\pi^+$, $\overline{\nu} p \to \mu^+ p\pi^-$

Table 7: Values of χ^2 per degree of freedom (NDF)
for the comparison of the theoretical predictions and the data
for the modified *Adler* model A including PCAC
and the alternative model D with a 'conserved axial current' (CAC).

Q^2 region	physical quantity	χ^2/NDF (PCAC)	χ^2/NDF (CAC)
$Q^2 < 0.15$ GeV^2	Q^2 distribution (νp)	$1.44/3 = 0.48$	$29.98/3 = 9.99$
$Q^2 < 0.30$ GeV^2	Q^2 distribution $(\overline{\nu} p)$	$0.27/3 = 0.09$	$4.00/3 = 1.33$
$Q^2 < 0.40$ GeV^2	$\tilde{\rho}_{33}$ (νp)	$6.21/3 = 2.07$	$17.09/3 = 5.70$
$Q^2 < 0.40$ GeV^2	$\tilde{\rho}_{31}$ (νp)	$0.54/3 = 0.18$	$16.02/3 = 5.34$
$Q^2 < 0.40$ GeV^2	$\tilde{\rho}_{3-1}$ (νp)	$1.60/3 = 0.53$	$1.80/3 = 0.60$
$Q^2 < 0.40$ GeV^2	$a^{\nu}_{10}/a^{\nu}_{00}$ (νp)	$5.29/3 = 1.76$	$7.84/3 = 2.61$
sum of all analysed quantities		$15.35/18 = 0.85$	$76.73/18 = 4.26$

FIGURE CAPTIONS

1. Definition of the pion angles θ_π, ϕ_π in the CMS. The lepton plane is spanned by the lepton momenta $\overrightarrow{k_1}$ and $\overrightarrow{k_2}$.

2. W distributions for $W < 3$ GeV.

3. Q^2 distributions for $W < 1.4$ GeV; the black areas show the observed events with $p_p^L < 0.2$ GeV/c.

4. Q^2 distributions for $W < 1.4$ GeV and $p_p^L > 0.2$ GeV/c, compared to the predictions of the modified model, which are normalized to the data.

5. Q^2 distributions for $W < 1.4$ GeV and $p_p^L > 0.2$ GeV/c, compared to the absolute predictions of

   A: the modified model presented in this paper, including the *Dürr–Pilkuhn* 'off–mass–shell' corrections (thick solid line),

   B: the original *Adler* model (thin solid line),

   C: the model without 'off–mass–shell' corrections (i. e. $f^I_{\ell\pm\ \mathrm{off}} \equiv f^I_{\ell\pm\ \mathrm{on}}$, dotted line), and

   D: the model with a 'conserved axial current' (dashed line).

6. Different contributions to the Q^2 distributions, as predicted by the modified model A, for $W < 1.4$ GeV and $p_p^L > 0.2$ GeV/c

   α) from the $\mathcal{L}$ multipoles, determined by PCAC,

   β) from the remaining axial–vector parts and

   γ) from the vector parts.

7. Contributions of the pion–nucleon angular momentum states $\ell\pm = 1+, 0+, 1-$ to the predicted Q^2 distributions in the modified model A, for $W < 1.4$ GeV and $p_p^L > 0.2$ GeV/c.

8. Experimental W distributions compared to the predictions of the modified model A, which are normalized to the data.

9. Density matrix elements of the $\Delta^{++}(1232)$ resonance in the neutrino reaction ($1a$) for $W < 1.4$ GeV, compared to the predictions of the modified model A (solid line) and the alternative model D with a 'conserved axial current' (dashed line).

10. Moments $a_{10}^{\nu}, a_{11}^{\nu}, b_{11}^{\nu}, b_{21}^{\nu}, b_{22}^{\nu}$ in the neutrino reaction $(1a)$ for $W < 1.4$ GeV, compared to the predictions of the modified model A (solid line) and the alternative model D with a 'conserved axial current' (dashed line).

11. Q^2 distributions for $W < 1.4$ GeV and $p_p^L > 0.2$ GeV/c, compared to the predictions of the modified model. The shaded areas show the uncertainty of the theoretical prediction corresponding to one standard deviation.

12. Experimental values and absolute predictions for the differential cross-sections $d\sigma^{\nu,\overline{\nu}}/dQ^2$ for $W < 1.4$ GeV. Shown are the predictions of the modified model A (solid line) and the alternative model D with a 'conserved axial current' (dashed line).

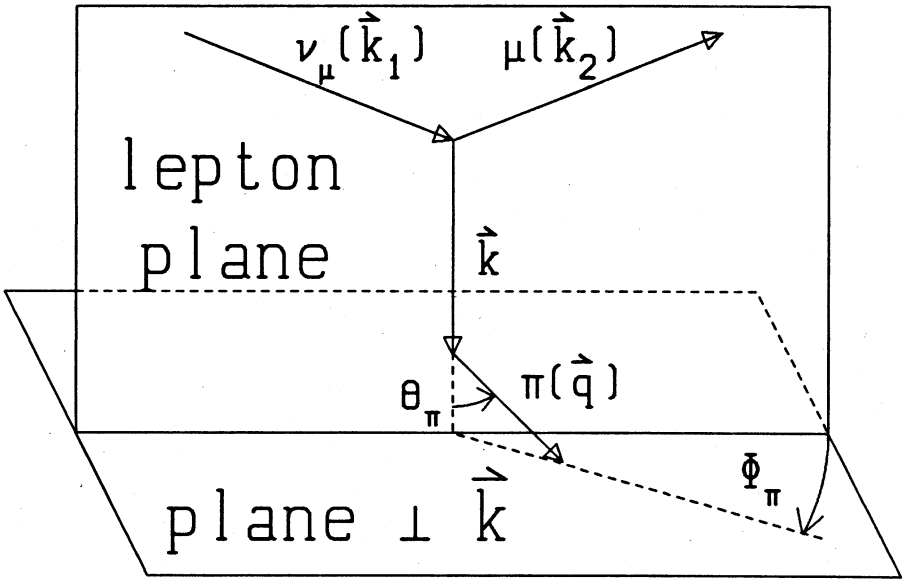
$\nu_\mu(\vec{k}_1)$
$\mu(\vec{k}_2)$
lepton
plane
$\vec{k}$
θ_π
$\pi(\vec{q})$
Φ_π
plane $\perp$ $\vec{k}$

Fig. 1

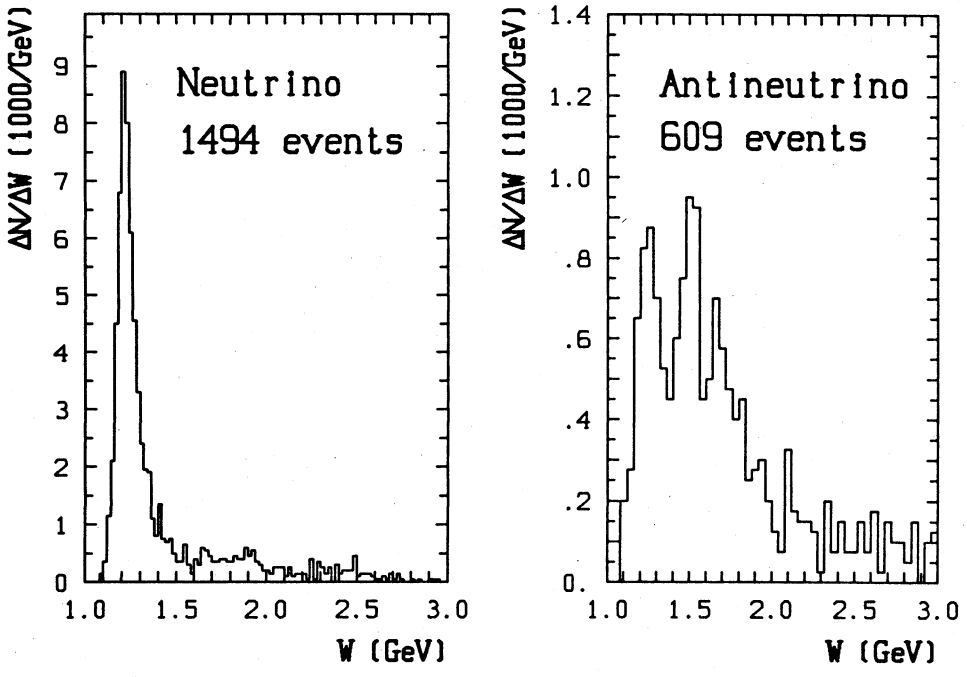
Neutrino
1494 events
ΔN/ΔW (1000/GeV)
W (GeV)
Antineutrino
609 events
ΔN/ΔW (1000/GeV)
W (GeV)

Fig. 2

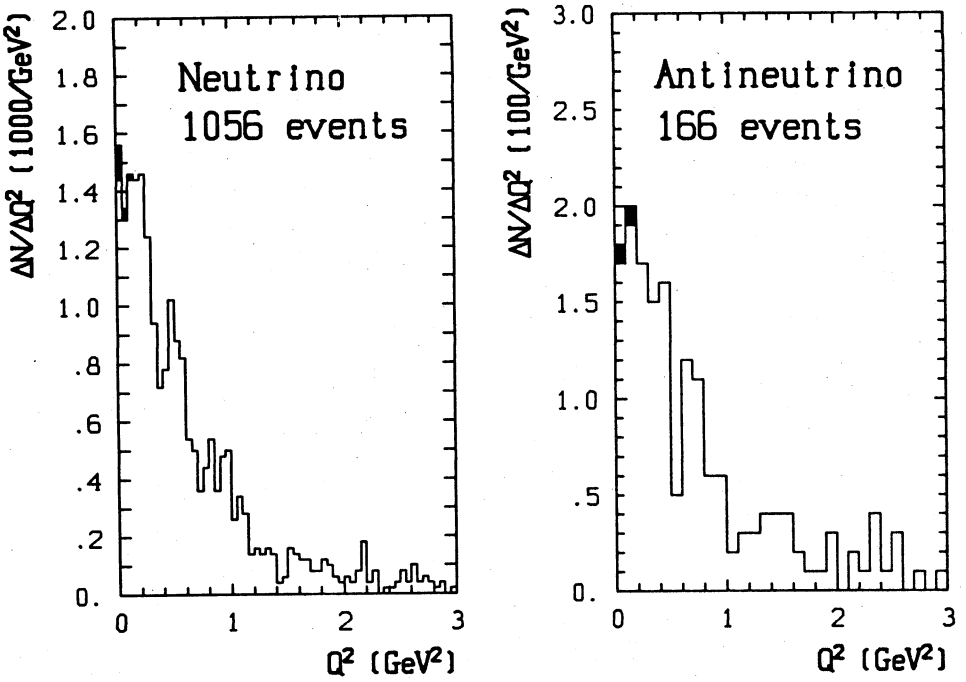
Neutrino
1056 events
Antineutrino
166 events
ΔN/ΔQ² (1000/GeV²)
ΔN/ΔQ² (100/GeV²)
Q² (GeV²)
Q² (GeV²)

Fig. 3

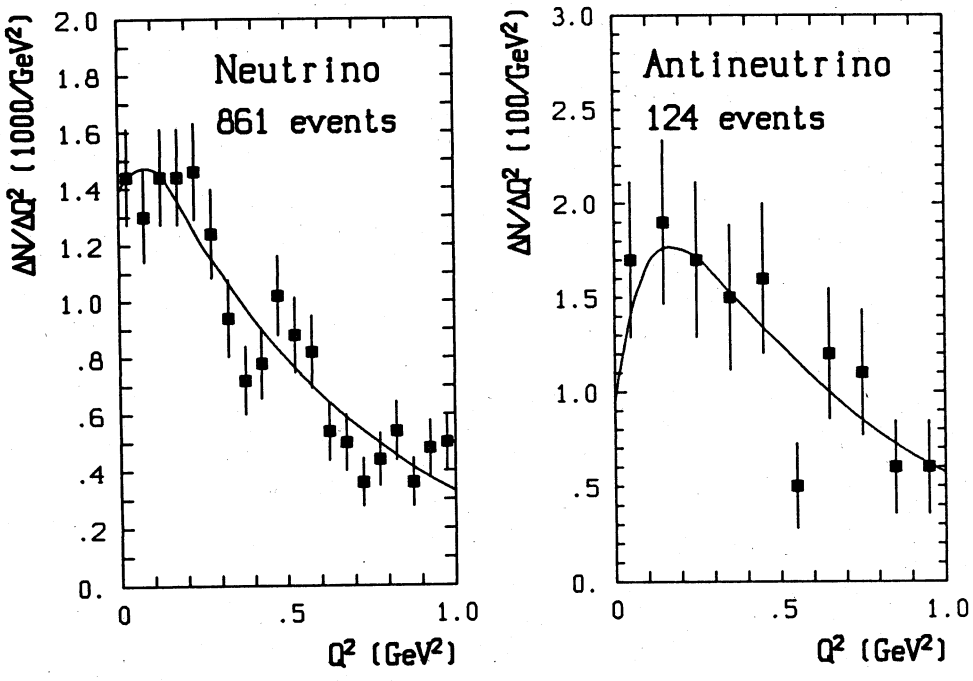
Neutrino
861 events
Antineutrino
124 events
ΔN/ΔQ² (1000/GeV²)
ΔN/ΔQ² (100/GeV²)
Q² (GeV²)
Q² (GeV²)

Fig. 4

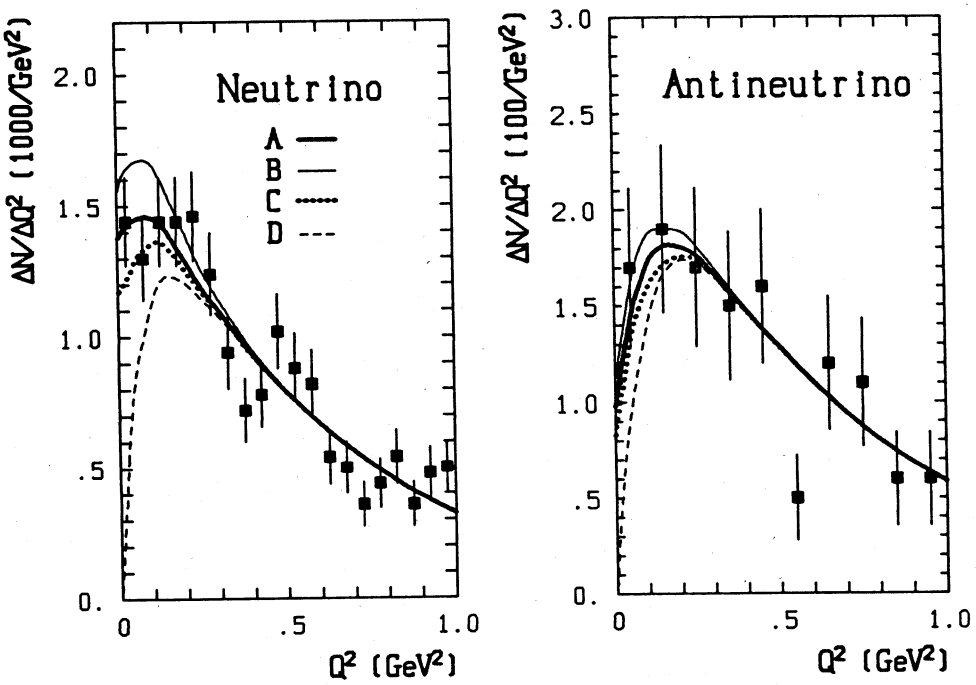
Neutrino
A
B
C
D
ΔN/ΔQ² (1000/GeV²)
Q² (GeV²)
Antineutrino
ΔN/ΔQ² (100/GeV²)
Q² (GeV²)

Fig. 5

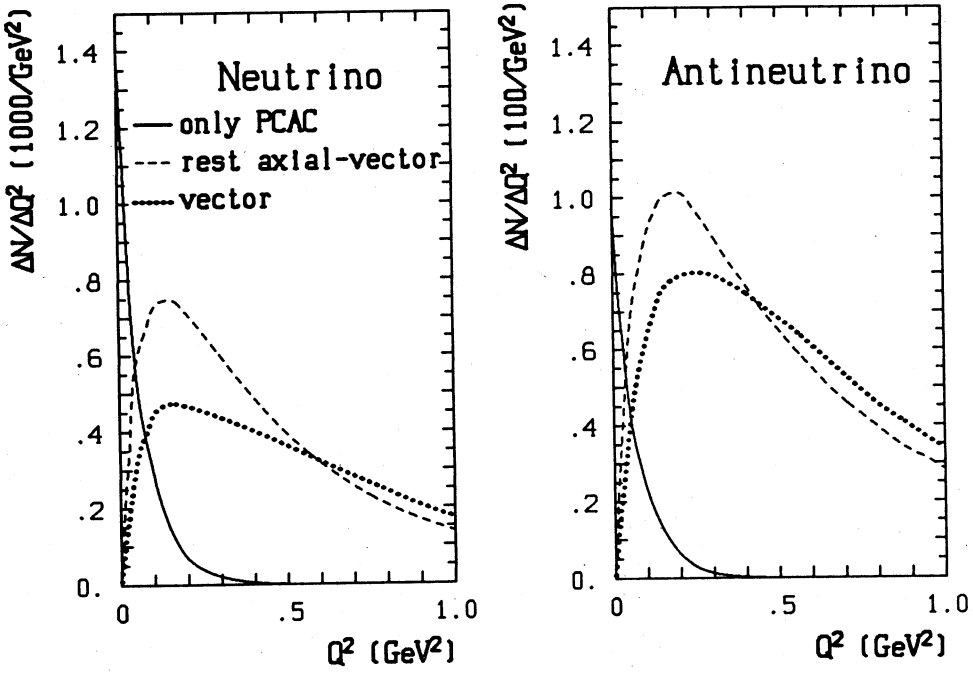
Neutrino
only PCAC
rest axial-vector
vector
ΔN/ΔQ² (1000/GeV²)
Q² (GeV²)
Antineutrino
ΔN/ΔQ² (100/GeV²)
Q² (GeV²)

Fig. 6

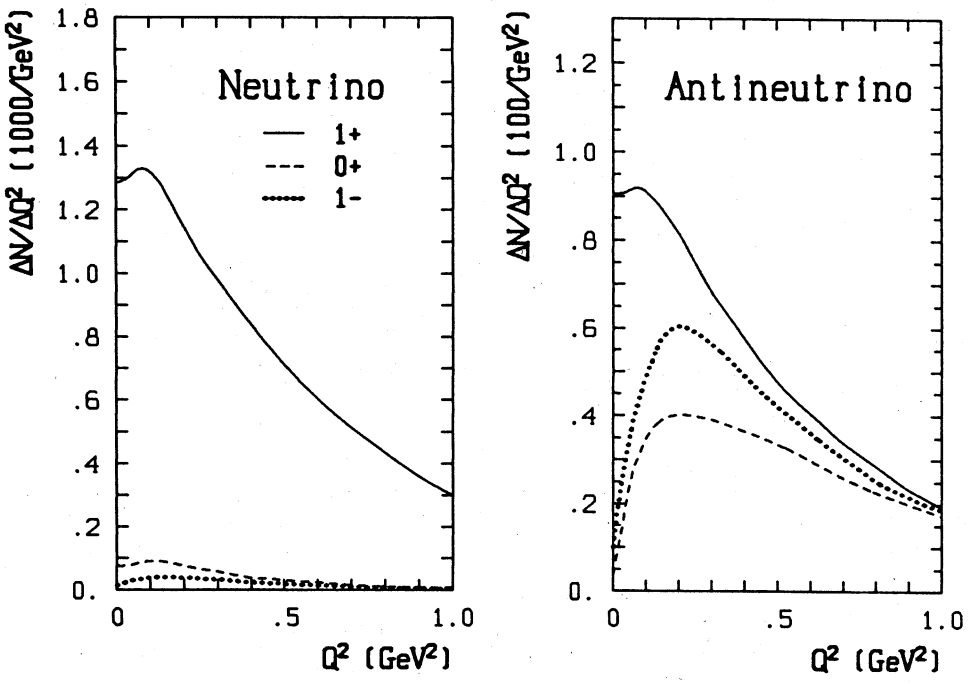
Neutrino
1+
0+
1-
ΔN/ΔQ² (1000/GeV²)
Q² (GeV²)
Antineutrino
ΔN/ΔQ² (100/GeV²)
Q² (GeV²)

Fig. 7

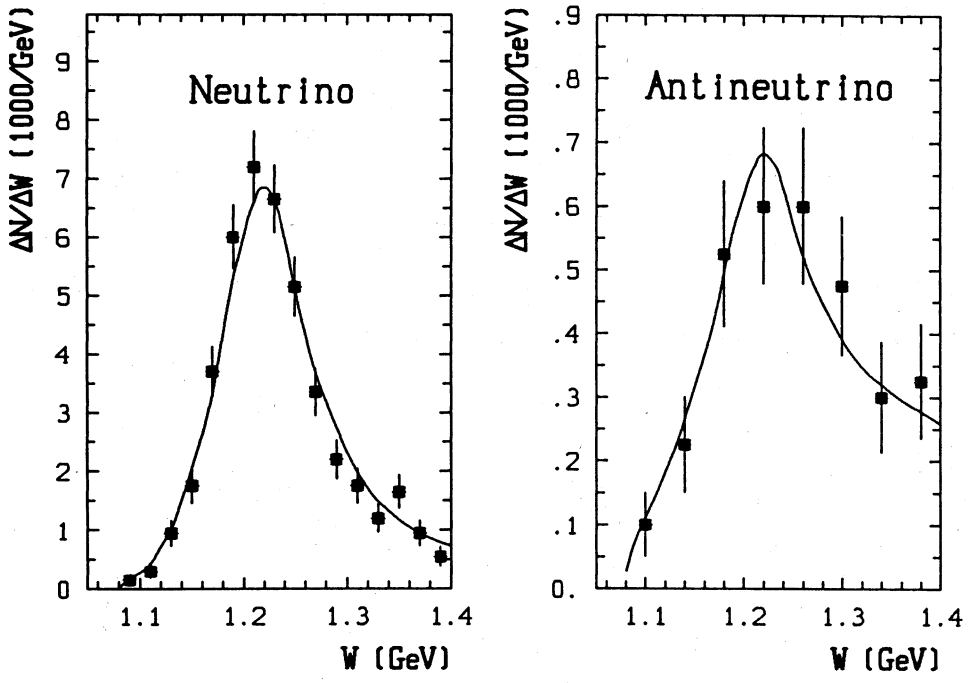
Neutrino
ΔN/ΔW (1000/GeV)
W (GeV)
Antineutrino
ΔN/ΔW (1000/GeV)
W (GeV)

Fig. 8

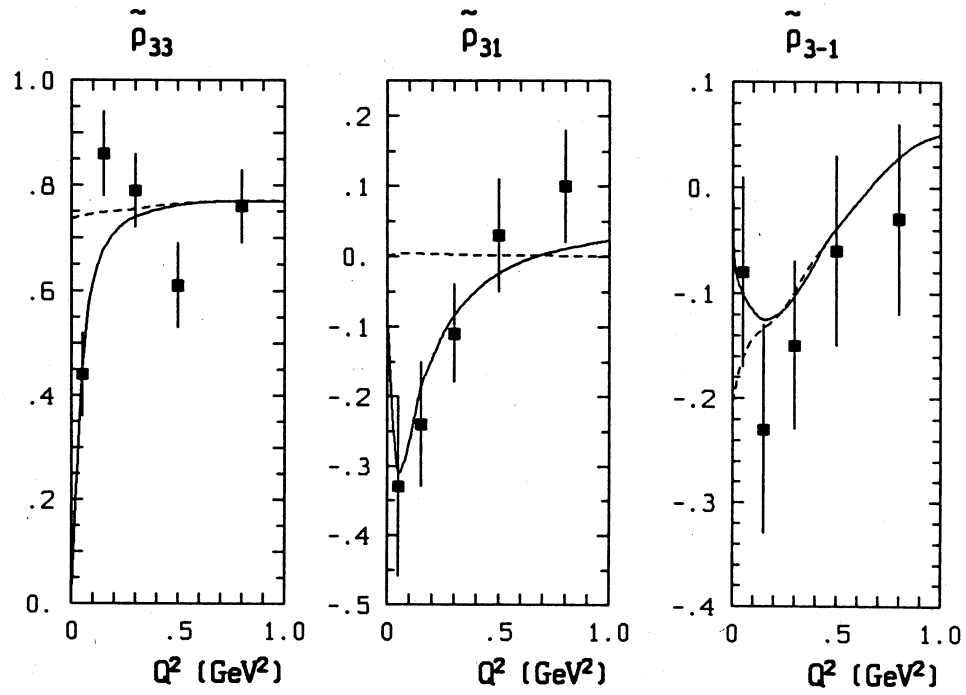
$\tilde{\rho}_{33}$
$\tilde{\rho}_{31}$
$\tilde{\rho}_{3-1}$
Q^2 (GeV^2)
Q^2 (GeV^2)
Q^2 (GeV^2)

Fig. 9

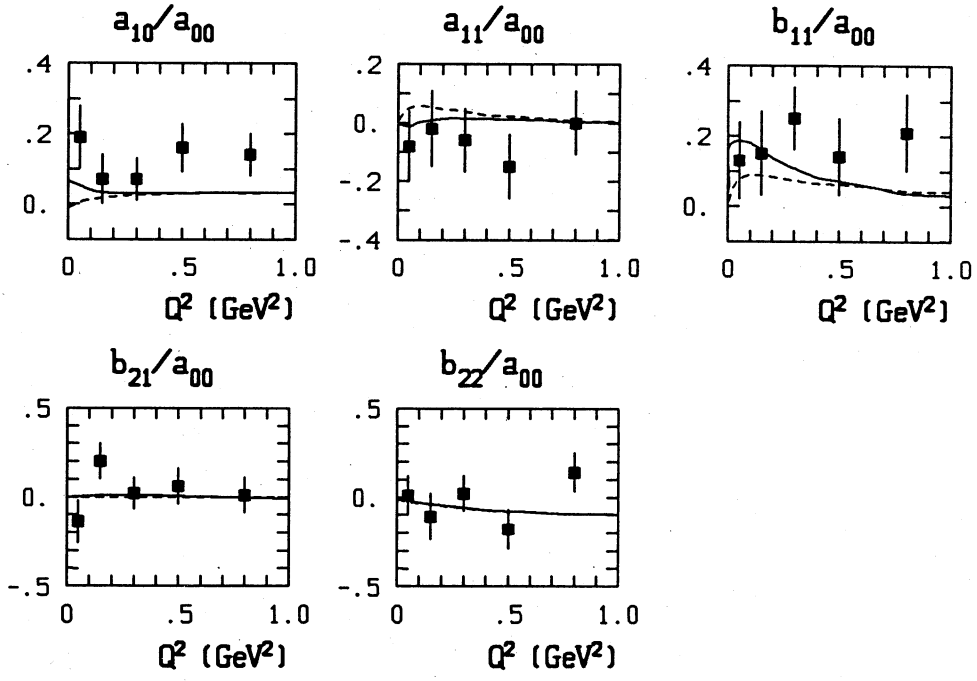
a_{10}/a_{00}
a_{11}/a_{00}
b_{11}/a_{00}
b_{21}/a_{00}
b_{22}/a_{00}
Q^2 (GeV^2)

Fig. 10

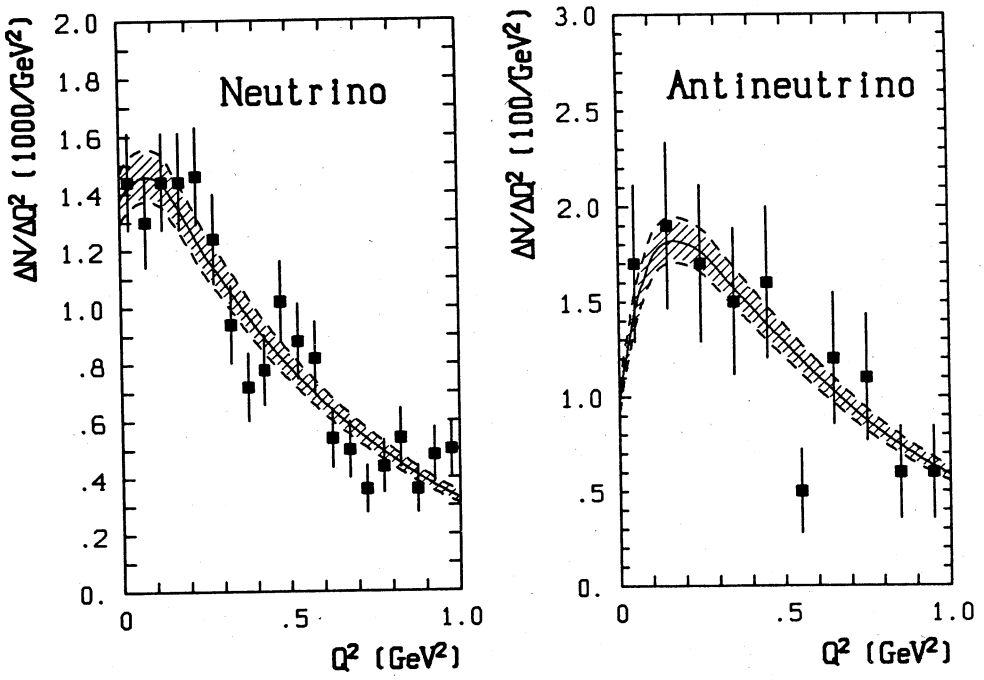
Neutrino
Antineutrino
ΔN/ΔQ² (1000/GeV²)
ΔN/ΔQ² (100/GeV²)
Q² (GeV²)
Q² (GeV²)

Fig. 11

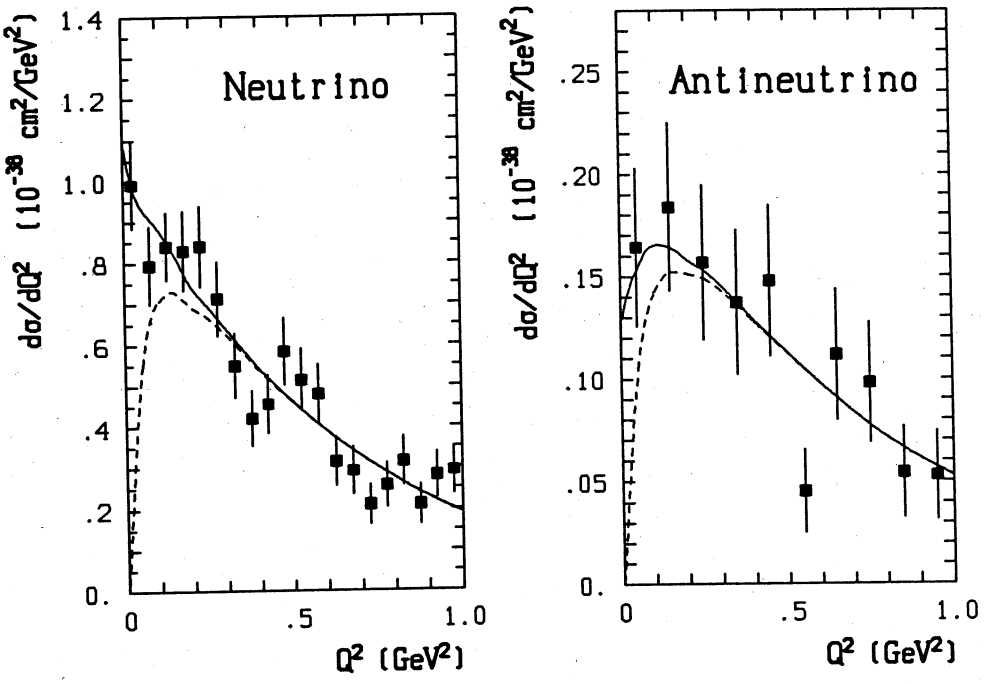
Neutrino
Antineutrino
dσ/dQ² (10⁻³⁸ cm²/GeV²)
dσ/dQ² (10⁻³⁸ cm²/GeV²)
Q² (GeV²)
Q² (GeV²)

Fig. 12